



# Nature of the Diffuse Source and Its Central Point-like Source in SNR 0509–67.5

Katrina C. Litke<sup>1,2</sup>, You-Hua Chu<sup>1,3</sup>, Abigail Holmes<sup>1</sup>, Robert Santucci<sup>1</sup>, Terrence Blindauer<sup>1</sup>, Robert A. Gruendl<sup>1</sup>, Chuan-Jui Li<sup>3,4</sup>, Kuo-Chuan Pan<sup>5,6</sup>, Paul M. Ricker<sup>1</sup>, and Daniel R. Weisz<sup>7</sup>

<sup>1</sup> Astronomy Department, University of Illinois, 1002 W. Green Street, Urbana, IL 61801, USA

<sup>2</sup> Now at Steward Observatory, University of Arizona, 933 N. Cherry Ave, Tucson, AZ 85721, USA; [klitke@email.arizona.edu](mailto:klitke@email.arizona.edu)

<sup>3</sup> Academia Sinica Institute of Astronomy and Astrophysics, P.O. Box 23-141, Taipei 10617, Taiwan, R.O.C.

<sup>4</sup> Institute of Astrophysics, Department of Physics, National Taiwan University, Taipei 10617, Taiwan, R.O.C.

<sup>5</sup> Departement Physik, Universität Basel, Klingelbergstrasse 82, CH-4056 Basel, Switzerland

<sup>6</sup> Now at Department of Physics and Astronomy, Michigan State University, East Lansing, MI 48824, USA

<sup>7</sup> Department of Astronomy, University of California, 501 Cambell Hall #3411, Berkeley, CA 94720-3411, USA

Received 2016 December 1; revised 2017 January 20; accepted 2017 January 23; published 2017 March 8

## Abstract

We examine a diffuse emission region near the center of SNR 0509–67.5 to determine its nature. Within this diffuse region we observe a point-like source that is bright in the near-IR, but is not visible in the *B* and *V* bands. We consider an emission line observed at 6766 Å and the possibilities that it is Ly $\alpha$ , H $\alpha$ , and [O II]  $\lambda$ 3727. We examine the spectral energy distribution (SED) of the source, comprised of *Hubble Space Telescope* *B*, *V*, *I*, *J*, and *H* bands in addition to *Spitzer*/IRAC 3.6, 4.5, 5.8, and 8  $\mu$ m bands. The peak of the SED is consistent with a background galaxy at  $z \approx 0.8 \pm 0.2$  and a possible Balmer jump places the galaxy at  $z \approx 0.9 \pm 0.3$ . These SED considerations support the emission line’s identification as [O II]  $\lambda$ 3727. We conclude that the diffuse source in SNR 0509–67.5 is a background galaxy at  $z \approx 0.82$ . Furthermore, we identify the point-like source superposed near the center of the galaxy as its central bulge. Finally, we find no evidence for a surviving companion star, indicating a double-degenerate origin for SNR 0509–67.5.

*Key words:* ISM: individual objects (SNR 0509–67.5) – ISM: supernova remnants – Magellanic Clouds

## 1. Introduction

Type Ia supernovae (SNe Ia) are often used as standardizable candles for cosmological distance indicators. This type of supernova (SN) occurs when a white dwarf in a binary system explodes. However, these standardizable candles are not completely understood. There are at least two theories for the origin of SNe Ia: single-degenerate and double-degenerate. A double-degenerate SN occurs when two white dwarfs merge (Iben & Tutukov 1984; Webbink 1984), while a single-degenerate SN is caused by a WD accreting material from a non-degenerate companion star (Whelan & Iben 1973; Nomoto 1982). In the double-degenerate origin, both stars are annihilated. In the single-degenerate origin, the non-degenerate companion star survives (Marietta et al. 2000; Pan et al. 2010, 2012).

We can study the remnants of SNe Ia to constrain the progenitor type. If a surviving companion star is identified in a Type Ia supernova remnant (SNR), the progenitor of the SN was single-degenerate. If there is no surviving companion star, a double-degenerate origin is more likely. By studying Type Ia SNRs and determining their progenitor types, SNe Ia can be better understood, especially in the context of standardizable candles.

In the Galaxy, three Type Ia SNRs have been searched for surviving companions: SN1006 (González Hernández et al. 2012; Kerzendorf et al. 2012), SN1572 (i.e., Tycho’s SN; Ruiz-Lapuente et al. 2004; González Hernández et al. 2009; Kerzendorf et al. 2009), and SN1604 (i.e., Kepler’s SN; Kerzendorf et al. 2014), but no surviving companions have been unambiguously identified. Few Type Ia SNRs are known in the Milky Way, thus an extended survey for surviving companions is not possible.

We can then turn to the Large Magellanic Cloud (LMC) to study Type Ia SNRs. The LMC is ideal for this research because it is at a known 50 kpc distance, is close enough for individual stars to be resolved, and is nearly face-on, limiting line-of-sight confusion. Twelve Type Ia SNRs have been reported in the LMC based on Balmer-line-dominated optical spectra, abundances of SN ejectra revealed by X-ray spectra, or even optical spectra of their SN light echos (Tuohy et al. 1982; Mathewson et al. 1983; Hughes et al. 1995; Borkowski et al. 2006; Seward et al. 2006; Rest et al. 2008; Maggi et al. 2014; A. Rest et al. 2016, in preparation). Therefore, we have started a program to study a subset of the Type Ia SNRs in the LMC to search for surviving companions using *Hubble Space Telescope* (*HST*) observations. In this paper we report our analysis of SNR 0509–67.5, one of the three smallest Type Ia SNRs in the LMC (i.e. Helder et al. 2010; di Stefano & Kilic 2012).

SNR 0509–67.5 has been studied extensively in the past. It is a Balmer-line-dominated young SNR (Tuohy et al. 1982), and its age determined from the SN light echoes is approximately  $400 \pm 120$  yr (Rest et al. 2005). Its H $\alpha$  shell in Figure 1 shows a simple and regular shape with a radius of approximately 16", or 4 pc, although the western side of the shell exhibits multiple parallel filaments along the shell rim, indicating that the SNR has run into a denser medium not as uniform as in the east.

Schaefer & Pagnotta (2012) examined *HST* images of SNR 0509–67.5 for possible surviving companion stars and concluded that it has no plausible candidate surviving companion and thus a double-degenerate origin. They also noted a patch of faint nebulosity near the center of SNR 0509–67.5. They postulated that the nebula was probably a background galaxy, but due to its position it could be associated with the explosion itself. After analyzing the *V*-band image, they also concluded that there were no point sources embedded within the nebula.

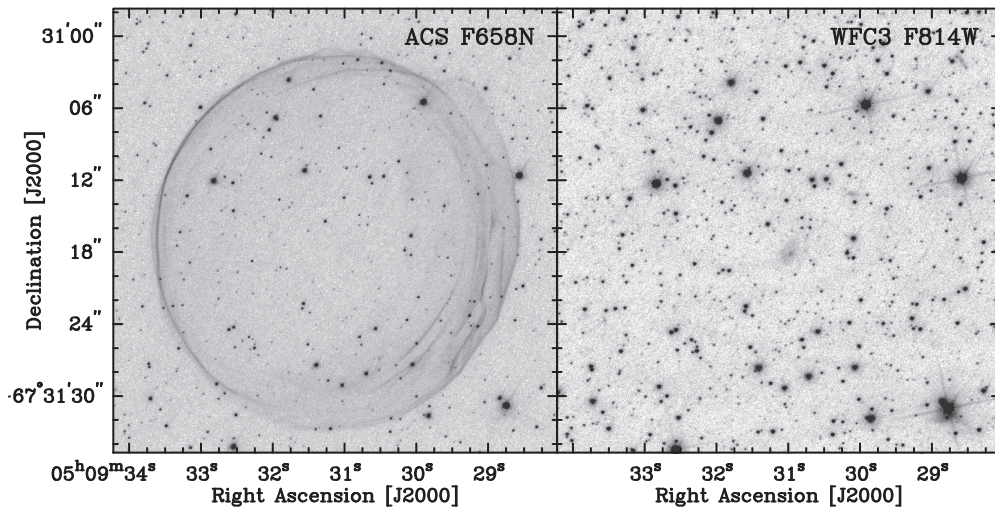


**Figure 1.** *HST* images of SNR 0509–67.5 in  $H\alpha$  (F658N) and  $I$  (F814W) bands. The camera and filter used for the images are labeled in the upper right corners.

In a follow-up study, Pagnotta et al. (2014) obtained a Gemini GMOS spectrum of the central patch of nebulosity in SNR 0509–67.5. The long-slit spectrum detected the  $H\alpha$  emission from the SNR itself, and an emission line at  $\lambda = 6766 \text{ \AA}$  from the central nebulosity. They argued that the observed  $6766 \text{ \AA}$  line must be a redshifted  $H\alpha$  line and that the central nebulosity originates from a background galaxy at  $z = 0.031$ .

Parallel to the work of Pagnotta et al. (2014), we have carried out an independent investigation of SNR 0509–67.5 and the diffuse region within. While the *HST*  $B$ - and  $V$ -band images do not show point sources in the diffuse patch, in the  $I$  band we noticed a point-like source near the center of the diffuse patch of emission (Figure 1). This source appears redder than the diffuse patch. This point-like source is of great interest because of its location near the SNR center.

In order to further investigate the nature of the point-like source and diffuse emission, we have acquired deeper *HST*  $I$  band observations. We have also acquired  $J$  and  $H$  band observations from *HST* to expand the wavelength coverage of SNR 0509–67.5 and construct spectral energy distributions (SEDs) for the diffuse region and point-like source. In addition, we have used *Spitzer* Space Telescope Infrared Array Camera (IRAC) data to extend the SEDs to longer wavelengths.

This paper reports our analysis of the diffuse source and the point-like source within. We describe the observations and data reduction in Section 2. In Section 3 we discuss the morphology of the diffuse source and discuss the SED of the emission patch. We then examine the emission line observed by Pagnotta et al. (2014) in Section 4. We identify the observed emission line and the nature of the diffuse patch in SNR 0509–67.5 in Section 5, and the nature of the point-like source in Section 6. We examine stars near the explosion center in Section 7. A summary is given in Section 8.

## 2. Data and Observations

Using the *HST* we obtained new  $J$  and  $H$  band images as well as follow-up  $I$  band images via Program 13282 (PI: Chu). All three images were taken using the Wide Field Camera 3 (WFC3) on 2013 September 24.

The F110W ( $J$ ) and F160W ( $H$ ) images used the IR-UVIS channel of WFC3. Both observations had a  $136'' \times 123''$  field

of view. The pixel size was  $0''.13$ , which corresponds to  $0.032 \text{ pc}$  at  $50 \text{ kpc}$ , the distance to the LMC. The F110W observation had two exposures, 99.2 and 198.5 s. The F160W observation had a 797.7 s total exposure time. The F110W and F160W observations were dithered using POSTARG.

The UVIS1 channel of WFC3 was used for the F814W ( $I$ ) image. The UVIS pixel size is  $0''.04$ , corresponding to  $0.01 \text{ pc}$  in the LMC. The observations were taken in three exposures, two 400 s exposures and one 600 s exposure. The FLASH = 3 option was used for the two 400 s exposures. For the 600 s exposure no pre-flash was needed; the background should have been high enough to mitigate the charge transfer efficiency effects in WFC3. The F814W observation was dithered using POSTARG offsets optimized for sub-pixel sampling.

In addition, archival *HST* data were available for the F475W ( $B$ ), F555W ( $V$ ), and F658N ( $H\alpha$ ) passbands. Archival *Spitzer*/IRAC images at 3.6, 4.5, 5.8, and  $8.0 \mu\text{m}$  were also utilized in our analysis. Details for the new and archival data are given in Table 1.

The *HST* data were downloaded from the Mikulski Archive for Space Telescopes. The photometry was determined using the DOLPHOT package. Magnitudes and uncertainties calculated from the fluxes are given in Table 2. The uncertainties listed are statistical and do not take into account the accuracy of flux calibration itself. The magnitudes are determined using the AB magnitude system (Oke 1974).

The *Spitzer* images cannot resolve the point-like source from the diffuse patch; therefore, the photometry was made with a large aperture to include both sources in all passbands for both *HST* and *Spitzer* data. We downloaded the *Spitzer*/IRAC BCD products from the *Spitzer* Heritage Archive and combined them to form a composite image for each of the four IRAC bands. Photometric measurements were then obtained using the IRAF package PHOT.

We first used DOLPHOT (for *HST* images) and the IRAF package PHOT (for *Spitzer* images) to find the peak of emission for the aperture center (i.e., floating aperture) and made measurements. The emission peak in the *Spitzer*  $5.8 \mu\text{m}$  image is ill-defined and appears offset from the emission peak at 3.6 and  $4.5 \mu\text{m}$ ; thus we made another measurement with the aperture center fixed to coordinates of the emission peak at 3.6 and  $4.5 \mu\text{m}$ . The two measurements yield different results because of the poor detection quality in the  $5.8 \mu\text{m}$  band; both

**Table 1**  
*HST* and *Spitzer* Data

Band	PI	Proposal #	Instrument	Channel	Date	Exp. (s)
F475W	Knoll	12326	<i>HST</i> /WFC3	UVIS2-FIX	2010 Nov 04	1010
F555W	Knoll	12326	<i>HST</i> /WFC3	UVIS2-FIX	2010 Nov 04	696
F658N	Hughes	11015	<i>HST</i> /ACS/WFC	WFC2	2006 Oct 28	4620
F656N	Hughes	11015	<i>HST</i> /WFPC2	WF3-fix	2007 Nov 07	14300
F814W	Chu	13282	<i>HST</i> /WFC3	UVIS1	2013 Sep 24	1465
F110W	Chu	13282	<i>HST</i> /WFC3	IR-UVIS	2013 Sep 24	298
F160W	Chu	13282	<i>HST</i> /WFC3	IR-UVIS	2013 Sep 24	798
3.6 $\mu\text{m}$	Borkowski	3680	<i>Spitzer</i> /IRAC	Channel 1	2004 Dec 19	10 $\times$ 30
4.5 $\mu\text{m}$	Borkowski	3680	<i>Spitzer</i> /IRAC	Channel 2	2004 Dec 19	10 $\times$ 30
5.8 $\mu\text{m}$	Borkowski	3680	<i>Spitzer</i> /IRAC	Channel 3	2004 Dec 19	10 $\times$ 30
8.0 $\mu\text{m}$	Borkowski	3680	<i>Spitzer</i> /IRAC	Channel 4	2004 Dec 19	10 $\times$ 30

results are reported in Table 2. The *Spitzer* 8.0  $\mu\text{m}$  value is a  $3\sigma$  lower limit for the magnitude, corresponding to an upper limit in the flux, and is not a detection.

Separate photometric measurements of the point-like source are made in the *I*, *J*, and *H* bands, and the results are also reported in Table 2. The aperture sizes used to make measurements are discussed further in Section 3.2.

To examine stars in the field of SNR 0509–67.5 we have also performed point-spread function photometry on each of the *HST* images using DOLPHOT, a version of HSTPHOT (Dolphin 2000) with *HST*-specific modules. We adopted photometric parameters following the recommendations of Williams et al. (2014). We filtered the detected object catalog to include only well-measured stars by only considering objects with a SNR  $> 5$ , sharp<sup>2</sup>  $< 0.1$ , and crowd  $< 1.0$ , again following the recommendations of Williams et al. (2014). Definitions of each of these parameters can be found in Dolphin (2000).

### 3. The Central Diffuse Emission Region and the Point-like Source

#### 3.1. Morphology

Near the central region of SNR 0509–67.5 is a diffuse patch of emission, as seen in Figure 1. This diffuse patch is visible in continuum images, but not detected in the  $H\alpha$  image. Figure 2 shows its closeups in *HST* F475W (*B*), F555W (*V*), F658N ( $H\alpha$ ), F814W (*I*), F110W (*J*), and F116W (*H*), and *Spitzer* 3.6, 4.5, and 5.8  $\mu\text{m}$  bands. The diffuse emission patch has a slightly oblong shape, with a major axis of  $2''.0 \pm 0''.3$  and a minor axis of  $1''.5 \pm 0''.3$ . Near the center of the diffuse patch is a point-like source.

The point-like source is best seen in Figure 3, where zoomed-in views in *HST* F814W (*I*), F110W (*J*), and F116W (*H*) are presented. The F814W image shows a sharp core within the central  $0''.1$  radius surrounded by a  $0''.55 \times 0''.4$  halo of raised surface brightness with an elongation similar in shape and direction to the entire diffuse emission region. A tracing of the surface brightness in F814W along the major axis is plotted in Figure 4. It can be seen that the surface brightness of the halo around the core is about two to three times as high as the extended diffuse emission region. In the F110W and F116W images, with poorer point-spread-functions (PSFs), the core and halo detected in the F814W image blend together into a point-like source slightly broader than the PSF.

#### 3.2. SEDs of Diffuse Region and Point-like Source

To diagnose the physical nature of the diffuse emission patch and its central point-like source, we carried out photometric measurements and constructed SEDs, using *HST* images in the F475W (*B*), F555W (*V*), F814W (*I*), F110W (*J*), and F160W (*H*) bands, and *Spitzer*/IRAC images in the 3.6, 4.5, 5.8, and 8.0  $\mu\text{m}$  bands. Depending on the instrumental resolution, different apertures were used to determine the flux at each wavelength as described below.

We first determine the total fluxes from the diffuse patch and the point-like source within, using a large aperture to include all of the light from both sources. The PSF in the *Spitzer*/IRAC bands has an FWHM of  $1''.7\text{--}2''$  (Fazio et al. 2004). We have thus used an aperture with radius  $3''.6$  for all passbands, and plotted the results in red squares in Figure 5. The images in Figure 2 show that within this aperture the emission is dominated by the central diffuse patch with no noticeable contributions from background stars in the IRAC bands, but does include significant emission from many bright background stars in the *HST* bands. Therefore, we repeated photometric measurements in the *HST* bands using a  $1''.05$  radius aperture that is just large enough to encompass the diffuse emission region without including any of the background stars. These measurements are plotted in black triangles in Figure 5. The SED of the total fluxes from the diffuse patch and the point-like source should thus consist of the black triangles below 2  $\mu\text{m}$  (*HST* bands) and red squares above 2  $\mu\text{m}$  (*Spitzer*/IRAC bands).

For the point-like source observed within the diffuse region, we use smaller apertures to exclude light from the diffuse region itself. We have considered both a  $0''.25$ -radius aperture and  $0''.1$  radius aperture. The  $0''.25$  aperture includes both the entirety of the point-like source and the aforementioned halo around it as seen in the F814W image (Figure 3) and surface brightness profile (Figure 4). The  $0''.1$  aperture excludes the halo, but includes only partial fluxes from the point-like source in the F110W and F160W bands. We have plotted the fluxes in  $0''.25$  aperture with green circles and  $0''.1$  aperture with blue crosses in Figure 5, but the interpretation of these measurements need to consider the above caveat. The point-like source is not detected in the *B* (F475W) or *V* (F555W) bands. It is not resolved in the *Spitzer*/IRAC data.

### 4. Emission Line at 6766 Å

In the diffuse region at the center of SNR 0509–67.5, Pagnotta et al. (2014) detected a single emission line at 6766 Å

**Table 2**  
Photometry of Diffuse Patch and Point-like Source

Pass Band	Diffuse Patch + Point Source	Point-like Source	Diffuse Patch
F475W ( <i>B</i> Band)	$24.15 \pm 0.05$	not detected	n/a
F555W ( <i>V</i> Band)	$23.99 \pm 0.06$	not detected	n/a
F814W ( <i>I</i> Band)	$21.95 \pm 0.02$	$25.22 \pm 0.04$	$22.00 \pm 0.02$
F110W ( <i>J</i> Band)	$21.27 \pm 0.01$	$23.04 \pm 0.04$	$21.50 \pm 0.02$
F160W ( <i>H</i> Band)	$20.73 \pm 0.01$	$22.40 \pm 0.03$	$20.99 \pm 0.01$
$3.6 \mu\text{m}$	$20.05 \pm 0.07$	not resolved	n/a
$4.5 \mu\text{m}$	$20.52 \pm 0.11$	not resolved	n/a
$5.8 \mu\text{m}$ (floating aperture)	$20.37 \pm 0.34$	not resolved	n/a
$5.8 \mu\text{m}$ (fixed aperture)	$20.67 \pm 0.43$	not resolved	n/a
$8.0 \mu\text{m}$ ( $3\sigma$ lower limit)	$>20.65$	not resolved	n/a

in addition to the  $H\alpha$  from the SNR itself. We will examine four possible identifications for the observed emission:  $\text{Ly}\alpha$ ,  $H\alpha$ ,  $[\text{O III}] \lambda 5007$ , and  $[\text{O II}] \lambda 3727$  (the  $\lambda\lambda 3726, 3729$  doublet). Because hydrogen is the most abundant element in the universe, we begin with hydrogen emission from  $\text{Ly}\alpha$  and  $H\alpha$  as the two brightest hydrogen recombination lines. After hydrogen and helium, oxygen is the next most abundant element in the universe, so we consider the brightest oxygen emission lines,  $[\text{O III}] \lambda 5007$  and  $[\text{O II}] \lambda 3727$ .

The brightest emission line that we would expect to see is  $\text{Ly}\alpha$ . If this line is  $\text{Ly}\alpha$ , the diffuse region is a background galaxy at a redshift of  $z \approx 4.6$ .

The next brightest emission line we would expect to observe is  $H\alpha$ . If this observed line is  $H\alpha$ , the diffuse region is a galaxy at  $z \approx 0.031$ , as Pagnotta et al. (2014) concluded. We would also expect to see the  $[\text{N II}] \lambda\lambda 6548, 6583$  doublet with the  $H\alpha$  line in a distinctive pattern. At  $z \approx 0.031$ , these lines would be at  $6744 \text{ \AA}$  and  $6781 \text{ \AA}$ , respectively. We observe only one line, not three as we would expect if this emission line was  $H\alpha$ . As the  $[\text{O III}] \lambda 5007$  line at  $z \sim 0.031$  is not detected (Pagnotta et al. 2014), the ionized gas must have low ionization and the  $[\text{N II}] \lambda 6583$  line should be bright; furthermore, if the warm ionized gas has a metallicity comparable to the solar neighborhood, the  $[\text{N II}] \lambda 6583$  line can be as bright as the  $H\alpha$  line (Haffner et al. 1999). The missing  $[\text{N II}]$  emission cannot be explained.

The next brightest line that we would expect is  $[\text{O III}] \lambda 5007$ . The  $[\text{O III}] \lambda\lambda 4959, 5007$  and the  $H\beta$  lines also form a distinctive pattern. While the corresponding  $[\text{O III}] \lambda 4959$  line happens to fall in a spectral gap, the non-detection of corresponding  $H\beta$  cannot be explained.

Finally, we consider  $[\text{O II}] \lambda 3727$ . Balmer lines near this wavelength are from higher-level transitions (e.g., the Balmer lines  $\lambda 3735$  and  $\lambda 3723$  originate from  $13 \rightarrow 2$  and  $14 \rightarrow 2$  transitions, respectively), and are thus weaker and not detected. If the emission line is  $[\text{O II}] \lambda 3727$ , the diffuse region is a background galaxy at  $z \approx 0.82$ .

From the above consideration, we eliminate the  $[\text{O III}] \lambda 5007$  and will further evaluate the other three possible identifications for the line:  $\text{Ly}\alpha$ ,  $H\alpha$ , and  $[\text{O II}] \lambda 3727$ . These three emission lines would place the diffuse patch as galaxies at redshifts of  $z \approx 4.6, 0.031$ , and  $0.82$ , respectively.

### 5. Nature of the Diffuse Patch of Emission at Center of SNR 0509–67.5

The identification of the emission line detected from the diffuse emission at the center of SNR 0509–67.5, combined with the photometry of the diffuse emission, places constraints on its

nature as a background galaxy. We have used Ned Wright’s Cosmology Calculator (Wright 2006) to determine expected physical properties of background galaxy at redshifts  $4.6, 0.031$ , and  $0.82$  that correspond to the  $\text{Ly}\alpha$ ,  $H\alpha$ , and  $[\text{O II}]$  identifications of the  $6766 \text{ \AA}$  feature, respectively. We adopt the parameters  $H_0 = 70$ ,  $\Omega_M = 0.3$ , and  $\Omega_{\text{vac}} = 0.7$  for these calculations.

If this emission line is  $\text{Ly}\alpha$  at  $z \approx 4.6$ , the diffuse patch would be a background galaxy with radius  $13.1 \pm 2.3 \text{ kpc}$  and  $M_J \sim -26.91 \pm 0.04$  (or  $\sim 10^{12.1} L_\odot$ ). This luminosity rivals those of ultraluminous IR galaxies (ULIRGs), but the SED of the diffuse patch peaks near  $2 \mu\text{m}$ , instead of mid- to far-IR. If the observed emission line is  $H\alpha$  at a redshift of  $z \approx 0.031$ , the diffuse patch is a dwarf galaxy with radius  $1.2 \pm 0.2 \text{ kpc}$  and  $M_J \sim -14.45 \pm 0.04$  (or  $\sim 10^{7.1} L_\odot$ ). If the emission line is  $[\text{O II}] \lambda 3727$  at  $z \approx 0.82$ , the diffuse patch would be a galaxy with radius  $15.1 \pm 2.0 \text{ kpc}$  and  $M_J \sim -22.35 \pm 0.04$  (or  $\sim 10^{10.3} L_\odot$ ), similar to our Milky Way Galaxy. We consider the latter two possibilities more viable.

The SED of the diffuse region (Figure 5) can place further constraint on the nature of the diffuse patch (Massarotti et al. 2001). The SED peaks at  $\lambda \approx 2.0 \pm 0.2 \mu\text{m}$ . For a normal galaxy, the SED peaks at  $\lambda \approx 1.1 \pm 0.1 \mu\text{m}$  in its rest frame (Polletta et al. 2007). The optical-IR SED of the diffuse region also resembles that of the bulge of M31, peaking near  $1.0 \mu\text{m}$  (Groves et al. 2012). Assuming that the diffuse region in SNR 0509–67.5 has a similar SED as normal galaxy or bulge of M31, its peaking at  $2.0 \pm 0.2 \mu\text{m}$  implies a redshift of  $z \approx 0.8 \pm 0.2$ , consistent with the  $[\text{O II}] \lambda 3727$  identification of the emission line.

The SED of the diffuse region also shows a break between F555W and F814W bands. If this is associated with the Balmer Jump at  $3647 \text{ \AA}$  similar to that seen in the SED of M31’s bulge (Groves et al. 2012), the redshift would be  $0.9 \pm 0.3$ , also supporting the  $[\text{O II}]$  identification of the emission line from the patch.

Based on the above arguments, we conclude that the diffuse emission patch near the center of SNR 0509–67.5 is a Milky-Way-like background galaxy at  $z \sim 0.8$ .

### 6. The Point-like Source in the Diffuse Emission Region

A natural explanation of the point-like source and its surrounding halo would be a luminous nucleus and bulge at the center of the disk galaxy at  $z \sim 0.8$ , similar to other galaxies and nuclei imaged in galaxies at  $0.5 < z < 1.2$  (Schade et al. 1995; Steinbring et al. 2008). As this study was originally motivated by the search for a surviving companion of the SN progenitor white dwarf, we will examine the point-like source

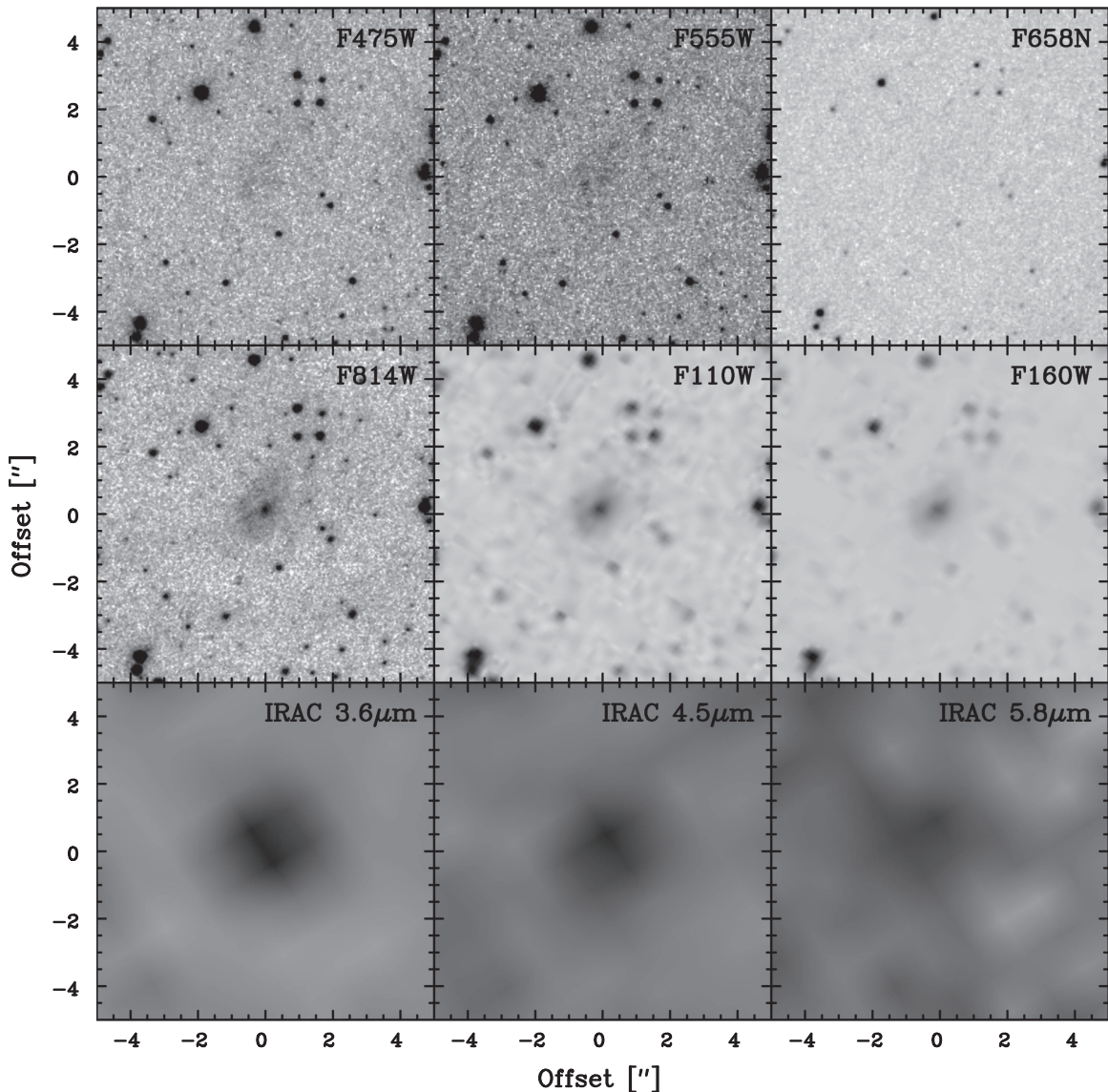


**Figure 2.** Central region of SNR 0509–67.5. From left to right, the top row: *HST* images in F475W (*B*), F555W (*V*), and F658N ( $H\alpha$ ); the middle row: *HST* images in F814W (*I*), F110W (*J*), and F160W (*H*); and the bottom row: *Spitzer*/IRAC images in 3.6, 4.5, and 8.0  $\mu\text{m}$ . The field of view of each panel is  $10'' \times 10''$ . The diffuse patch is detected in all broad continuum bands but not in the narrow  $H\alpha$  band. The point-like source is detected in the *I*, *J*, and *H* images (middle row).

and evaluate the possibility of its association with SNR 0509–67.5.

The point-like source is detected in *I*, *J*, and *H* bands, but it is blended with a small extended halo in the *J* and *H* bands. Only the *HST I* band image resolves the central source of the diffuse patch into a narrow core surrounded by a small halo (see Figure 4), allowing photometry of the point-like source with minimal background contamination. Using a  $1''.05$  radius aperture with aperture correction, we find  $I = 25.22 \pm 0.04$ ,  $J = 23.04 \pm 0.04$ , and  $H = 22.40 \pm 0.03$  for the point-like source. The colors of the point-like source,  $I - J = 2.18$ ,  $J - H = 0.64$ , and  $I - H = 2.82$ , are consistent with those of an M6 V star (Pecaut & Mamajek 2013). If this is an M6 V star with  $M_I = 12.47$ , its distance modulus would be 12.75 and distance  $\sim 3.5$  kpc. Such a distance is in the halo of the Milky Way, where stellar density is very low; thus it is unlikely that this point-like source is a foreground star in the halo of the

Milky Way. If this is a star in the LMC with distance modulus 18.5, its  $M_I \sim 6.72$ , too faint to be a giant. The colors and magnitudes of this point-like source will rule out most popular single-degenerate channels, including red-giant, sub-giant, main-sequence, and helium star channels (Pan et al. 2014). Therefore, this point-like source is unlikely to be a surviving star, unless it is originated from a peculiar single-degenerate channel.

While it is possible to make ad hoc assumptions to assign a single-star origin for the point-like source surrounded by a small halo at the center of the diffuse region, based on the principle of Occam’s razor we conclude that this point-like source is the bulge of a background galaxy at  $z \sim 0.8$ .

## 7. Stars Near the Explosion Center

Our original motivation to study the SNR 0509–67.5 is to search for a surviving companion of its SN progenitor. Using

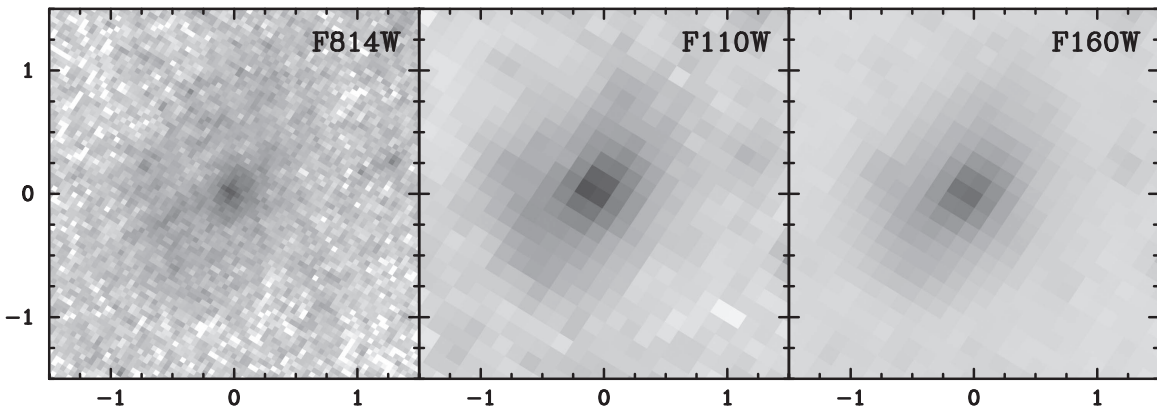


**Figure 3.** Zoomed-in views of the central diffuse emission region in SNR 0509–67.5. From left to right: *HST* images in F814W (*I*), F110W (*J*), and F160W (*H*) bands. The field of view of each panel is  $3'' \times 3''$ .

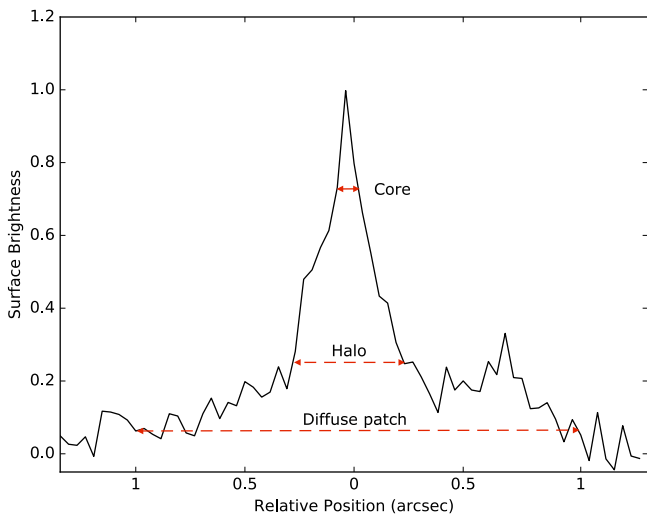


**Figure 4.** Surface brightness profile along the major axis of the diffuse patch near the center of SNR 0509–67.5 in the F814W band. The extents of core, halo, and the diffuse patch are marked.

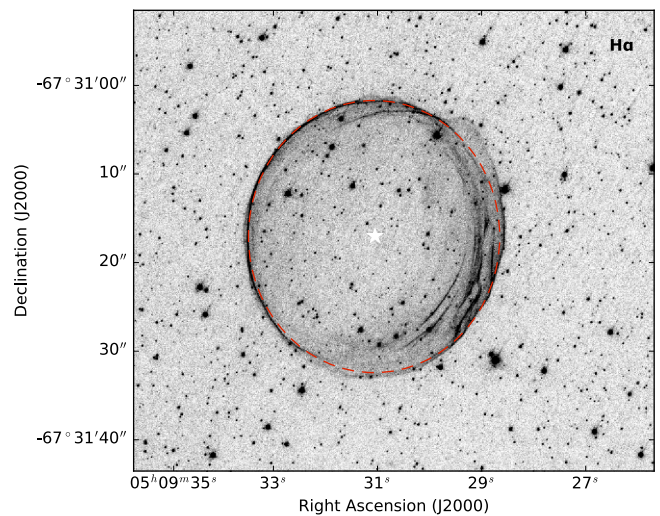


**Figure 6.** SNR 0509–67.5 with its center marked by a white star. The center was found by fitting an ellipse (the red dashed curve) to the SNR.

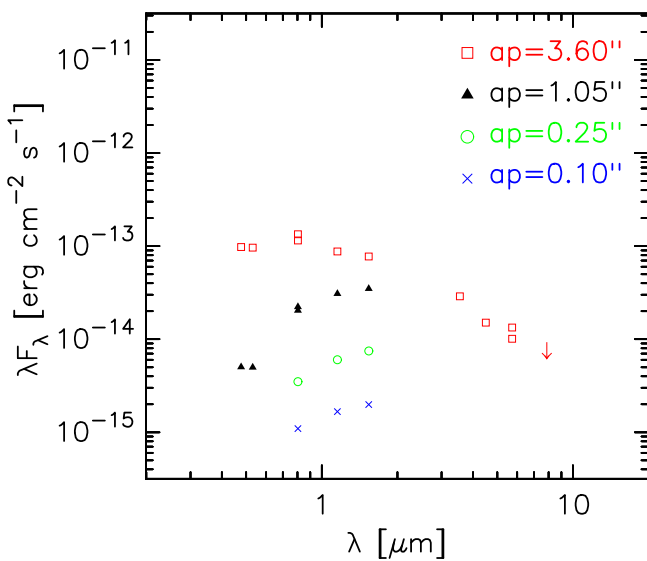


**Figure 5.** SED for the diffuse region in SNR 0509. From left to right, the bands shown are F475W (*B* band), F555W (*V* band), F814W (*I* band), F110W (*J* band), F160W (*H* band), and *Spitzer*/IRAC (the last three sets of points). Four different apertures were used to determine the fluxes.

our new *HST* observations, we reexamine the stars near the explosion center and compare them to models. The outer periphery of the  $H\alpha$  shell can be well fitted by an ellipse in three quadrants; only the northwest quadrant appears more extended, as shown in Figure 6. We assume that this northwest deviation is caused by some local anomaly and adopt the center of the ellipse as the explosion center, at  $5^{\text{h}}09^{\text{m}}31^{\text{s}}.15$ ,  $-67^{\circ}31'17''.1$  (J2000). This center is offset by  $1''.3$  from that adopted by Schaefer & Pagnotta (2012), at  $5^{\text{h}}09^{\text{m}}30^{\text{s}}.98$ ,  $-67^{\circ}31'17''.9$  (J2000). These two centers are marked in Figure 7 for comparison.

We have selected all stars within  $3''$  (or  $0.75$  pc) from our explosion center, and plotted them in the F555W versus F475W–F555W and F814W versus F555W–F814W color–magnitude diagrams (CMDs) in Figure 8. The  $3''$  radius is a generous limit of the search for surviving companion, as this would correspond to a kick velocity of  $1875 \text{ km s}^{-1}$  for an age of 400 yr. We have also plotted the post-impact evolutionary tracks of surviving companions from Pan et al. (2014). It is clear that no stars overlap the tracks of helium stars (the vertical tracks on the left of the CMDs), or tracks for companions stars with initial masses of  $0.93$ – $1.65 M_{\odot}$  (the curved tracks near the center of the CMDs). In fact, most stars appear to be normal main-sequence stars. The brightest star, corresponding to star L of Schaefer & Pagnotta (2012), has

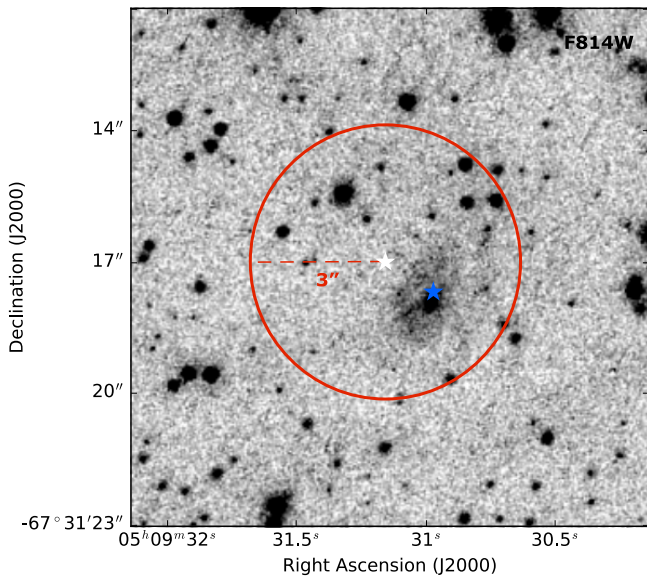


**Figure 7.** Center region of SNR 0509–67.5. The red circle denotes the area in which a surviving companion star would likely be found. The blue star,  $1''/3$  from the white star, is the center adopted by Schaefer & Pagnotta (2012).

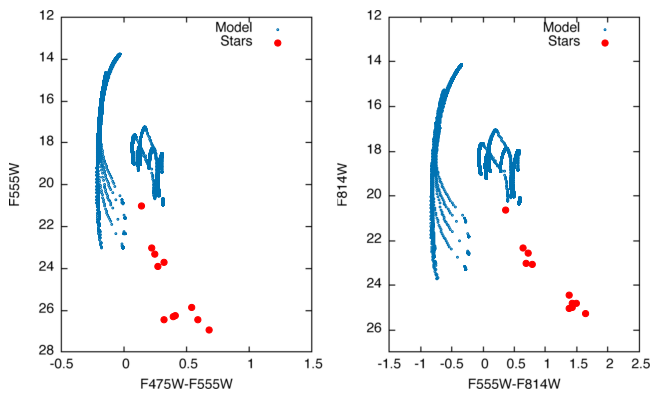


**Figure 8.** Color–magnitude diagrams for the stars in the center region of SNR 0509–67.5 (red), with theoretical post-impact evolutionary tracks from Pan et al. (2014) shown in blue. The group of tracks on the left are for helium star companions, and the group of tracks near the center of the diagram are for main-sequence companions.

$V = 21.0$  and  $B - V = 0.14$ , consistent with an A5 V star in the LMC with negligible extinction. Although this star is close to the model tracks, it is  $1''/7$  (or  $0.425$  pc) from the explosion center, requiring a kick velocity of over  $1000 \text{ km s}^{-1}$ , which is very unlikely. Based on the above analysis, we conclude that no surviving normal companion stars are found, similar to the search by Schaefer & Pagnotta (2012).

## 8. Summary

In this paper, we discuss different possibilities for the origin of the diffuse source at the center of SNR 0509–67.5. Using *HST* and *Spitzer* photometric measurements, we construct an SED of the diffuse emission and the point-like source within. We also examine a Gemini GMOS spectrum of the central region, which shows an emission line at  $\lambda = 6766 \text{ \AA}$  and consider it jointly with the SED.

We consider four possibilities for the identity of this observed emission line. We reject [O III]  $\lambda 5007$  because  $H\beta$  was not observed. In the case of  $\text{Ly}\alpha$ , the luminosity of the corresponding background galaxy would be similar to that of a ULIRG, but the peak of the SED is not consistent with that of a ULIRG; this possibility is therefore unlikely. If the line is  $H\alpha$ , we expect the source to be a dwarf galaxy at  $z \approx 0.031$ . We finally consider [O II]  $\lambda 3727$ , placing the source at  $z \approx 0.82$ .

The location of the peak of the SED, compared with the SED of spiral galaxies or the bulge of M31, implies a redshift of  $z \approx 0.8 \pm 0.2$  for the source. A possible Balmer Jump in the SED also places the source at  $z \approx 0.9 \pm 0.3$ . Considering the SED with the possible identities of the emission line, we suggest that the emission line is [O II]  $\lambda 3727$ , and the source is a background galaxy at  $z \approx 0.8$ . This background galaxy has radius  $15.1 \pm 2.0 \text{ kpc}$  and luminosity  $10^{10.3} L_{\odot}$ , similar to the Milky Way Galaxy.

The point-like source at the center of the background galaxy has colors similar to those of M6 V stars, but it requires many ad hoc assumptions to make it a star associated with SNR 0509–67.5. Based on Occam’s razor, we suggest that the point-like source is the bulge of the background galaxy at  $z \approx 0.82$ .

Finally, we have examined the stars within  $3''$  from the explosion center of SNR 0509–67.5 and compared them with the expected post-impact evolutionary tracks of surviving companion stars. We confirm the results of Schaefer & Pagnotta (2012) that no surviving companion is found.

This project is supported by the NASA grant HST-GO-13282.01-A. K.C.L. acknowledges support from the U.S. National Science Foundation under grant No. AST-1312950. Y.H.C. and C.J.L. are supported by Taiwanese Ministry of Science and Technology grant MOST 104-2112-M-001-044-MY3.

## References

- Borkowski, K. J., Hendrick, S. P., & Reynolds, S. P. 2006, *ApJ*, 652, 1259  
 Di Stefano, R., & Kilic, M. 2012, *ApJ*, 759, 56  
 Dolphin, A. E. 2000, *PASP*, 112, 1383  
 Fazio, G. G., Hora, J. L., Allen, L. E., et al. 2004, *ApJS*, 154, 10  
 González Hernández, J. I., Ruiz-Lapuente, P., Filippenko, A. V., et al. 2009, *ApJ*, 691, 1  
 González Hernández, J. I., Ruiz-Lapuente, P., Tabernero, H. M., et al. 2012, *Natur*, 489, 533  
 Groves, B., Krause, O., Sandstrom, K., et al. 2012, *MNRAS*, 426, 892  
 Haffner, L. M., Reynolds, R. J., & Tufté, S. L. 1999, *ApJ*, 523, 223  
 Helder, E. A., Kosenko, D., & Vink, J. 2010, *ApJL*, 719, L140  
 Hughes, J. P., Hayashi, I., Helfand, D., et al. 1995, *ApJL*, 444, L81  
 Iben, I., Jr., & Tutukov, A. V. 1984, *ApJS*, 54, 335  
 Kerzendorf, W. E., Childress, M., Scharwächter, J., Do, T., & Schmidt, B. P. 2014, *ApJ*, 782, 27  
 Kerzendorf, W. E., Schmidt, B. P., Asplund, M., et al. 2009, *ApJ*, 701, 1665  
 Kerzendorf, W. E., Schmidt, B. P., Laird, J. B., Podsiadlowski, P., & Bessell, M. S. 2012, *ApJ*, 759, 7  
 Maggi, P., Haberl, F., Kavanagh, P. J., et al. 2014, *A&A*, 561, A76  
 Marietta, E., Burrows, A., & Fryxell, B. 2000, *ApJS*, 128, 615  
 Massarotti, M., Iovino, A., & Buzzoni, A. 2001, *A&A*, 368, 74  
 Mathewson, D. S., Ford, V. L., Dopita, M. A., et al. 1983, *ApJS*, 51, 345  
 Nomoto, K. 1982, *ApJ*, 253, 798  
 Oke, J. B. 1974, *ApJS*, 27, 21  
 Pagnotta, A., Walker, E. S., & Schaefer, B. E. 2014, *ApJ*, 788, 173  
 Pan, K.-C., Ricker, P. M., & Taam, R. E. 2010, *ApJ*, 715, 78  
 Pan, K.-C., Ricker, P. M., & Taam, R. E. 2012, *ApJ*, 750, 151

- Pan, K.-C., Ricker, P. M., & Taam, R. E. 2014, *ApJ*, 792, 71
- Pecaut, M. J., & Mamajek, E. E. 2013, *ApJS*, 208, 9
- Polletta, M., Tajer, M., Maraschi, L., et al. 2007, *ApJ*, 663, 81
- Rest, A., Matheson, T., Blondin, S., et al. 2008, *ApJ*, 680, 1137
- Rest, A., Suntzeff, N. B., Olsen, K., et al. 2005, *Natur*, 438, 1132
- Ruiz-Lapuente, P., Comeron, F., Méndez, J., et al. 2004, *Natur*, 431, 1069
- Schade, D., Lilly, S. J., Crampton, D., et al. 1995, *ApJL*, 451, L1
- Schaefer, B. E., & Pagnotta, A. 2012, *Natur*, 481, 164
- Seward, F. D., Williams, R. M., Chu, Y.-H., et al. 2006, *ApJ*, 640, 327
- Steinbring, E., Melbourne, J., Metevier, A. J., et al. 2008, *AJ*, 136, 1523
- Tuohy, I. R., Dopita, M. A., Mathewson, D. S., Long, K. S., & Helfand, D. J. 1982, *ApJ*, 261, 473
- Webbink, R. F. 1984, *ApJ*, 277, 355
- Whelan, J., & Iben, I., Jr. 1973, *ApJ*, 186, 1007
- Williams, B. F., Lang, D., Dalcanton, J. J., et al. 2014, *ApJS*, 215, 9
- Wright, E. L. 2006, *PASP*, 118, 1711